for a given element size at a specific surface location occurred as the tunnel speed was increased and the boundary-layer thickness was reduced. Many of the elements tested exhibited this behavior, with the downstream movement of transition starting at higher Re_k and k/δ as the element location approached the leading edge.

Acknowledgment

References

[1]Klebanoff, P. S., Schubauer, G. B., and Tidstrom, K. D., "Measurements of the Effect of Two-Dimensional and Three-Dimensional Roughness Elements on Boundary-Layer Transition," *Journal of the Aeronautical Sciences*, Vol. 22, No. 11, 1955, pp. 803, 804.

[2]Smith, A. M. O., and Clutter, D. W., "The Smallest Height of Roughness Capable of Affecting Boundary-Layer Transition," *Journal of the Aerospace Sciences*, Vol. 26, No. 4, 1959.

[3]Tani, I., Komoda, H., and Konatsu, Y., "Boundary-Layer Transition by Isolated Roughness," Rept. 375, Aeronautical Research Inst., Univ. of Tokyo, Japan, Nov. 1962.

[4]Braslow, A. L., Hicks, R. M., and Harris, R. V., "Use of Grit-Type Boundary-Layer-Transition Trips on Wind Tunnel Models," NASA TN D-3579, 1966.

[5]Morkovin, M. V., "Bypass Transition to Turbulence and Research Desiderata," NASA CP-2386, May 1984, pp. 161–204.

[6]Von Doenhoff, A. E., and Horton, E. A., "A Low-Speed Experimental Investigation of the Effect of a Sandpaper Type of Roughness on Boundary-Layer Transition," NACA Rept. 1349, 1956.

[7]Peterson, J. B., and Horton, E. A., "An Investigation of the Effect of a Highly Favorable Pressure Gradient on Boundary-Layer Transition as Caused by Various Types of Roughness on a 10-Foot-Diameter Hemisphere at Subsonic Speeds," NASA MEMO 2-8-59L, 1959.

[8]Cummings, M. J., "Airfoil Boundary-Layer Transition Due to Large Isolated 3-D Roughness Elements in a Favorable Pressure Gradient," M.S. Thesis, Univ. of Illinois at Urbana–Champaign, IL, 1995.

[9]Bragg, M. B., Kerho, M. F., and Cummings, M. J., "Airfoil Boundary Layer Due to Large Leading-Edge Roughness," AIAA Paper 95-0536, Jan. 1995.

[10]Shin, J., "Characteristics of Surface Roughness Associated with Leading Edge Ice Accretion," AIAA Paper 94-0799, Jan. 1994.

[11]Tani, I., "Effect of Two-Dimensional and Isolated Roughness on Laminar Flow," *Boundary Layer and Flow Control*, edited by G. V. Lachmann, Vol. 2, Pergamon, Oxford, England, UK, 1961, pp. 637–656.

Pressure Fluctuations in an Unstable Confined Jet

Patricia Ern* and José Eduardo Wesfreid†
Ecole Supérieure de Physique et Chimie Industrielles, 75231 Paris Cedex 05, France

Introduction

THIS Note reports on a study of pressure fluctuations at the exit of a two-dimensional jet confined in a rectangular cavity. Experimental observations were made for various Reynolds numbers and cavity lengths. The results show an initial weak oscillation at lower Reynolds numbers followed by a strong self-sustained oscillation regime at higher Reynolds numbers, eventually perturbed by a noisy background. The main findings of this Note are an amplitude hysteresis between the frequency stages and a transition in the flow type behavior from convectively unstable to absolutely unstable. For a selection of related works, the reader is referred to Refs. 1–10.

*Boursière Docteur Ingénieur, Laboratoire Physique et Mécanique des Milieux Hétérogènes, URA CNRS 857, 10, rue Vauquelin.

†Directeur de Recherches, Laboratoire Physique et Mécanique des Milieux Hétérogènes, URA CNRS 857, 10, rue Vauquelin.

Experimental Setup

The experimental configuration composed a gravity-driven water flow discharging into the horizontal cavity. The cavity (Fig. 1) was a parallelepipedic chamber 10 cm wide and 2.5 cm high. Its length L was selected by moving the right-hand end wall. At the middle height of the cavity, the jet had a uniform velocity profile over about 70% of its width. The Reynolds number Re was based on the inflow characteristics at the point of the expansion, i.e., nozzle width of 0.4 cm, mean velocity U_m obtained as the flow rate divided by a nozzle section 2.5×0.4 cm^2, and a dynamic viscosity of 1.05×10^{-3} Pa · s. The flow rate was regulated with two precision needle valve rotameters, placed after the jet chamber to avoid perturbations in the flow. Two rotameters, Vögtlin V100-300 09 and V100-300 12, of 1% accuracy were used. Errors in viscosity and velocity induced an error of approximately 5% on the Reynolds number.

A variable reluctance pressure transducer Validyne type DP-103-10-N1S4D was used. The detecting holes were placed at half of the height of the cavity and 0.2 cm away from the exit contraction corner, as shown in Fig. 1. The transducer was associated with a Validyne CD15 carrier demodulator (1-V output signal for 8.63-Pa differential pressure). This signal was sent to a Fourier analyzer Scientific-Atlanta SD380. The flow rate was varied in steps of 0.28 cm^3/s, in either increasing or decreasing sequences. At each step, once the flow was stabilized, 500 pressure-spectra samples were averaged. Visualization of the flow was performed simultaneously by injecting fluorescein dye. Results will be discussed for $L = 5$ cm and $L = 7$ cm, but for brevity, only the experiments for $L = 7$ cm will be shown in the figures.

Results and Discussion

Spectra Analysis and Nature of the Oscillations

Figure 2 shows several pressure spectra observed for $L = 7$ cm at different Reynolds numbers. For the longer cavities studied ($L \geq 6$ cm), the jet oscillation started at small flow rates ($Re \sim 160$) with a low-frequency f_L lying in the $\sim$0.3–0.4 Hz range. The oscillation at this frequency had a small amplitude, and the spectrum also contained harmonics, notably, $2f_L$. As the Reynolds number was increased, these peaks grew and broadened. This broad spectrum is characteristic of a convective instability in open flows.[11] For a specific flow rate ($Re \sim 210$) that depended on the cavity length the spectrum suddenly concentrated on one sharp peak f_1 of a considerably higher amplitude. It seemed that the feedback was then synchronized with the instability wave, thus corresponding to self-sustained oscillating behavior.[12] Such an abrupt change in the peak width is similar to that observed by Babcock et al.[13] for a Taylor–Couette experiment with an axial flow.

In previous studies just using visualization methods,[14,15] it was shown that only time-periodic discrete frequencies could be observed and could be associated with different integer modes n, scaling L to the wavelength λ according to the well-known Brown–Curle[16–18] phenomenological relation[2,3] $\lambda = L/(n + \frac{1}{4})$. In Fig. 2, the intense peak at frequency f_1 for $Re \sim 210$ corresponds to the wavelength of mode $n = 3$ for $L = 7$ cm ($n = 2$ for $L = 5$ cm). As the Reynolds number was increased, the frequency f_1 increased
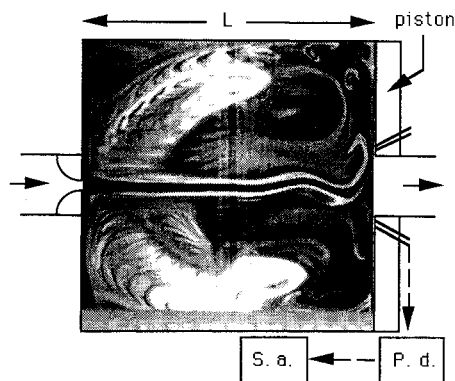

Fig. 1 Cavity geometry and differential pressure detection: pressure detector (P.d.) and spectrum analyzer (S.a.).
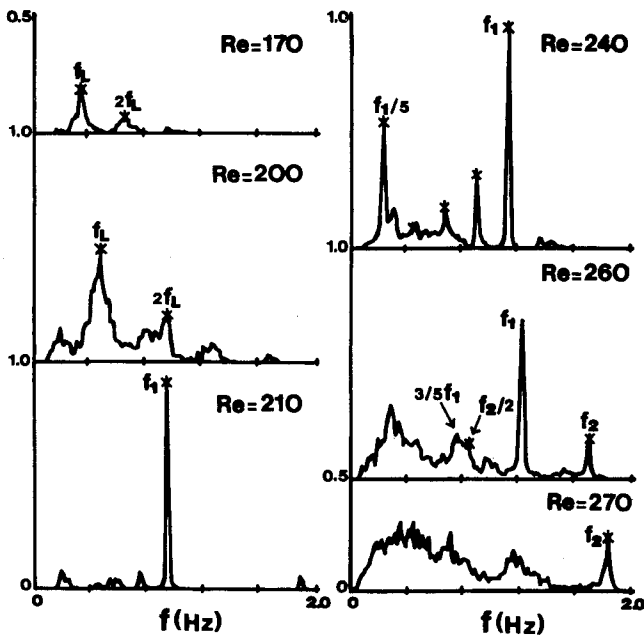
Fig. 2 Example of a sequence of differential pressure spectra for several Reynolds numbers for $L = 7$ cm; in the vertical scale, 1.0 corresponds to 0.44 Pa.
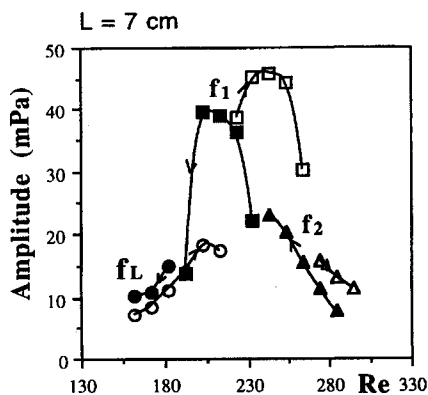

Fig. 3 Amplitudes (mPa) of major peaks, for increasing (open symbols) and decreasing (filled symbols) Reynolds numbers: circles, frequency f_L; squares, frequency f_1 and triangles, frequency f_2.

linearly in the range ~ 0.8–1.2 Hz for $L = 7$ cm. The spectrum also showed subharmonic multiples of $\frac{1}{5}$ for $L = 7$ cm ($\frac{1}{3}$ for $L = 5$ cm) of considerable amplitude. Some flow rates also exhibited either intermittent switching or coexistence[3] between f_1 and a second frequency f_2. Frequency switching was observed in instantaneous samplings (every 0.9 s) by the growth of a frequency and its decay, followed by the same behavior for the competing frequency. Frequency f_2 in Fig. 2 corresponds to the second stage of the self-sustained oscillation of wavelength mode $n = 4$ for $L = 7$ cm ($n = 3$ for $L = 5$ cm). After further increasing the Reynolds number, only frequency f_2 was observed. Its amplitude, however, was low, and the spectrum also presented broad low-frequency peaks. Depending on the Reynolds number, the frequency range observed for f_2 was ~ 1.4–1.9 Hz for $L = 7$ cm. As function of the Reynolds number, the values of the Strouhal number, $Sr = fL/U_m$, can be grouped in bands corresponding to the different modes of given n (upper limit $n = 4$ for the cavity lengths considered). For the same Reynolds number, several branches can be present simultaneously. For instance, frequencies $3f_1/5$ and f_1 for $L = 7$ cm are in the Strouhal number bands $n = 2$ and $n = 3$, respectively.

We have also compared the amplitudes of the stages between sequences of increasing/decreasing Reynolds numbers. The results are presented in Fig. 3, where the open symbols correspond to an increasing sequence and the filled symbols to a decreasing sequence. Figure 3 shows the existence of an hysteresis. In the case of f_L, the

difference between amplitudes is lower (half the one for f_2) with amplitudes higher for the decreasing velocity sequence. This could be consistent with the noise amplifier character of the instability at small Reynolds numbers. At high Reynolds numbers, when the decreasing velocity sequence is started, the difference in amplitudes might be explained by the fact that the energy was spread over a larger number of frequencies.

Discussion

We suggest that, in our configuration, the jump between stages is realized via the smallest possible frequency jump. For instance, we observed that the peak at f_1 seemed to be generated by the peak at $2f_L$, as we also observed an energy shift from the peak at $3f_1/5$ for $L = 7$ cm ($2f_1/3$ for $L = 5$ cm) to the peak at $f_2/2$. These transitions appear to occur around Strouhal number bands of constant n. When the spectra exhibited particular subharmonics, we also observed by dye visualization[19] that the jet presented at the exit a deviation from the centerline[6] (that can be thought as a $\lambda = 4L$ mode) and an additional recirculation region. The size of this additional hydrodynamical loop can be considered as the cavity length for an additional mode. We relate the subharmonics to the presence of the recirculation and suggest that an effective hydrodynamic feedback produces the subharmonics. Future work should include a detailed analysis of the multiple-frequency regions.

Acknowledgments

References

[1]Powell, A., "On the Edgetone," Journal of the Acoustical Society of America, Vol. 33, No. 4, 1961, pp. 395–409.

[2]Hussain, A., and Zaman, K., "The Free Shear Layer Tone Phenomenon and Probe Interference," Journal of Fluid Mechanics, Vol. 87, No. 2, 1978, pp. 349–383.

[3]Rockwell, D., and Naudascher, E., "Self-Sustained Oscillations of Impinging Free Shear Layers," Annual Review of Fluid Mechanics, Vol. 11, 1979, pp. 67–94.

[4]Ho, C.-M., and Nosseir, N. S., "Dynamics of an Impinging Jet. Part 2: The Noise Generation," Journal of Fluid Mechanics, Vol. 116, Aug. 1982, pp. 379–391.

[5]Kaykayoglu, R., and Rockwell, D., "Unstable Jet-Edge Interaction. Part 2: Multiple Frequency Pressure Fields," Journal of Fluid Mechanics, Vol. 169, March 1986, pp. 151–172.

[6]Fearn, R. M., Mullin, T., and Cliffe, K. A., "Nonlinear Flow Phenomena in a Symmetric Sudden Expansion," Journal of Fluid Mechanics, Vol. 211, Feb. 1990, pp. 595–608.

[7]Yu, K. H., Trouvé, A., and Daily, J. W., "Low-Frequency Pressure Oscillations in a Model Ramjet Combustor," Journal of Fluid Mechanics, Vol. 232, Nov. 1991, pp. 47–72.

[8]Fox, M. D., Kurosaka, M., Hedges, L., and Hirano, K., "The Influence of Vortical Structures on the Thermal Fields of Jets," Journal of Fluid Mechanics, Vol. 255, Oct. 1993, pp. 447–472.

[9]Broze, G., and Hussain, F., "Nonlinear Dynamics of Forced Transitional Jets: Periodic and Chaotic Attractors," Journal of Fluid Mechanics, Vol. 263, March 1994, pp. 93–132.

[10]Raman, G., and Rice, E. J., "Supersonic Jet Mixing Enhancement Using Impingement Tones from Obstacles of Various Geometries," AIAA Journal, Vol. 33, No. 3, 1995, pp. 454–462.

[11]Chomaz, J. M., Huerre, P., and Redekopp, L. G., "Bifurcations to Local and Global Modes in Spatially Developing Flows," Physical Review Letters, Vol. 60, No. 1, 1988, pp. 25–28.

[12]Huerre, P., and Monkewitz, P., "Local and Global Instabilities in Spatially Developing Flows," Annual Review of Fluid Mechanics, Vol. 22, 1990, pp. 473–537.

[13]Babcock, K., Ahlers, G., and Cannell, D., "Noise-Sustained Structure in Taylor-Couette Flow with Through Flow," Physical Review Letters, Vol. 67, No. 4, 1991, pp. 3388–3391.

[14]Maurel, A., "Instabilité d'un Jet Confiné," Ph.D. Thesis, Université Paris VI, France, July 1994.

[15]Wesfreid, J. E., Zielinska, B., Maurel, A., Ern, P., and Bouchet, G., "Oscillateur Fluidique: Application à la Débitmétrie des Ecoulements Monophasiques," La Houille Blanche, No. 7, 1994, pp. 99–104.

[16]Brown, G. B., "The Vortex Motion Causing Edge-Tones," Proceedings of the Physical Society, Vol. 49, Pt. 5, 1937, pp. 493–507.

[17]Brown, G. B., "The Mechanism of Edge-Tone Production," *Proceedings of the Physical Society*, Vol. 49, Pt. 5, 1937, pp. 508–521.

[18]Curle, N., "The Mechanics of Edge-Tones," *Proceedings of the Royal Society* A, Vol. 216, 1953, pp. 412–424.

[19]Ern, P., "Etude Expérimentale d'un Jet Confiné," Rapport de Diplôme d'Etudes Approfondies, Université Paris XI, Paris, France, June 1994.

Kármán Vortex Development: Relation to Symmetry and Circulation of Transition Vortices

C.-K. Chyu* and D. Rockwell[†]

Lehigh University, Bethlehem, Pennsylvania 18055

Introduction

AT sufficiently high Reynolds number, the shear layers separating from a cylinder exhibit well-defined, small-scale concentrations of vorticity that feed into the large-scale Kármán vortices. Bloor[1] and Gerrard[2] characterized various features of these small-scale structures and their consequence on the mean flow features of the near wake. This Bloor–Gerrard mechanism of transition is, for the range of Reynolds numbers of interest herein, essentially due to amplification of a thin shear-layer instability. Its overall character is that of a Kelvin–Helmholtz instability, but it is more explicitly described as a solution of the Rayleigh equation. The principal features of the small-scale shear-layer vortices, from both quasi-two-dimensional and three-dimensional perspectives, have been assessed.[3–11] The inherent instability frequency of these vortices and their control by application of external disturbances are clearly established in several of these investigations.

The issue arises as to how the rate of development and the symmetry of (i.e., phase shift between) small-scale vortices in opposing shear layers influence the location and form of the large-scale Kármán vortices formed in the near wake. Indeed, the shear-layer vortices do, in the end, comprise the Kármán vortices. These features are investigated using instantaneous images of vorticity.

Experimental System and Techniques

Experiments were carried out in a free-surface water channel. It had a square test section of 597×597 mm and a length of 4000 mm. The water level was maintained at a height of approximately 530 mm. A cylinder of diameter $D = 25.4$ mm was mounted horizontally at the middepth of the water channel; a vertical false wall isolated the cylinder support from the main flow through the test section. Details of this experimental arrangement are given by Chyu.[12] The freestream velocity was maintained at $U = 182$ mm/s, giving a value of Reynolds number of $Re = 5 \times 10^3$.

The instantaneous velocity field over the entire midplane of the cylinder was determined using a laser-scanning version of high-image-density particle image velocimetry (PIV). This approach is described by Rockwell et al.[13,14] and Rockwell and Lin.[15] The laser-scanning system involves an argon-ion (4-W) laser, which was deflected from a rotating mirror with 72 facets. The flow was seeded with 12-μm-diam hollow glass spheres coated with a thin layer of silver. Particle images were recorded on high-resolution 35-mm film via a Nikon F4 camera with a 105-mm lens. The lens system

has a magnification factor $M = 1:2.9$. Directional ambiguity was avoided by employing a bias mirror immediately in front of the camera lens. The 35-mm negatives were digitized at a high resolution of 125 pixels/mm, then interrogated at a window size 100×100 pixels with 50% overlap. The velocity vector corresponding to each interrogation window was obtained using a single-frame cross-correlation approach. The grid in the plane of the laser sheet had a spacing of 1.63 mm. The estimated uncertainties of the velocity and vorticity are approximately 0.5 and 4%, respectively.

Instantaneous and Averaged Vorticity Distributions and Streamline Patterns

Figure 1 shows images of vorticity distributions at instants of time 1, 2, and 3. The instantaneous images, which were acquired at a time interval corresponding to the period of Kármán vortex formation, are representative of the extreme states of the wake. The image of averaged vorticity was obtained from an ensemble average of the three instantaneous images. The intent of this averaged image is to demonstrate the lack of phase locking of the small-scale, shear-layer vortices during formation of successive Kármán vortices for a limited number of Kármán cycles. The blank region on the upper side of the cylinder is due to the shadow of the laser sheet in that region. The small-scale concentrations of vorticity represent the manifestations of the transition first identified by Bloor[1] and Gerrard.[2] The shear-layer vortices eventually agglomerate to form the large-scale Kármán vortex, indicated by the negative (bold white) region of vorticity extending across the entire wake in each of the three instantaneous images. At instant 1, a sequence of small-scale vortices, as many as three to five, are clearly evident in the upper and lower shear layers from the cylinder. The Kármán vortex has approximately an elliptical shape, and its major axis is oriented vertically. At instant 2, however, the development of the pattern of shear-layer vortices is not as consistent; in fact, there is an abrupt appearance of a relatively large-scale vortex in the upper shear layer. This development of the shear-layer system is associated with a Kármán vortex that is inclined at an angle of about 45 deg but still extends across the entire wake. Finally, the development of the shear-layer vortices at instant 3 occurs rapidly and in phase in both the upper and lower shear layers. That is, at a given streamwise location, the location and scale of the first three vortices are nearly mirror images of each other in the opposite shear layers. Moreover, the vorticity contour levels suggest that the second shear-layer vortices have rapidly attained a large value of circulation, relative to their counterparts in image 1. In this case, the Kármán vortex on the lower side forms relatively late and is inclined at a shallow angle, relative to instants 1 and 2. These three instantaneous images are representative of the extreme states of the wake over many Kármán cycles. The sequence of patterns shown in these images is, however, not generally repeatable.

The averaged image reveals that the detailed, instantaneous structure of the shear-layer vortices is essentially lost. Indications of the rate of development and phase between these small-scale concentrations of vorticity on opposite sides of the wake, so evident in images 1, 2, and 3, are not apparent in the averaged image. Moreover, inspection of the averaged contours of the Kármán vortex shows low levels, and therefore a small value of total circulation, relative to each of the instantaneous representations of the Kármán vortex. This is because the centroids of each of the instantaneous Kármán concentrations generally occur at markedly different locations in the instantaneous images, i.e., they are not phase locked to the Kármán formation.

Figure 2 gives values of circulation of the vortices for the instantaneous and averaged images. Rectangular boxes indicate the circuits employed for evaluation of the circulation $\Gamma^* = \Gamma/\pi U D$, in which Γ is circulation, U is freestream velocity and D is cylinder diameter. Viewing, first of all, the values of Γ^* for the shear-layer vortices, they typically have an initial value on the order of 0.1, but more mature concentrations show levels as high as the order of 0.2. The magnitude of Γ^* of the shear-layer vortices relative to the eventually formed Kármán vortices is of interest. In an attempt to establish this relationship, an approximate circuit is drawn around the large-scale agglomeration of image 1. It has a value of 0.79. We conclude that the vortices formed in the shear layer of image 1